Available online at www.sciencedirect.com

SCIENCE DIRECT®

Catalysis Today 105 (2005) 152–161

CATALYSIS TODAY

www.elsevier.com/locate/cattod

Structural characterization of Pt nanoclusters deposited on graphite: Effects of substrate and surrounding medium

Zhihui Gu, Perla B. Balbuena *

Department of Chemical Engineering, Texas A&M University, College Station, TX 77843, USA

Abstract

The structure of Pt_6, Pt_{13}, Pt_{20}, Pt_{40}, Pt_{60}, Pt_{100}, and Pt_{150} nanoparticles deposited on graphite surfaces, and the changes on such structures induced by the interactions with OH-terminated polyamidoamine dendrimers of the lowest generations G0OH and G1OH are examined using classical molecular dynamics simulations. It is shown that the particle/substrate interaction depends strongly on the particle size, with variations following an oscillatory pattern according to the degree of completeness of the particle's outer atomic shell. The results for the bare clusters suggest the existence of ordered structures with mixed fcc and hcp structures. Less ordered structures show a tendency of the nanoparticle to adopt a spherical shell. Details of the morphology and interactions of Pt_6, Pt_{13}, and Pt_{20} with the substrate in the presence of the dendrimers are compared with those for the bare nanoparticles deposited on graphite. Simulation results reveal a strong attachment of the dendrimer branches to the metal particle. The binding, which is driven by the oxygen and nitrogen amide atoms, the tertiary amines, and the dendrimer terminal groups, has significant effects on the structure of Pt nanoparticles on graphite surfaces, manifested by atomic rearrangements in the metal clusters causing modifications to their initial structure and the appearance of new layers.

Keywords: Dendrimers; Nanoclusters; Substrate

1. Introduction

Supported nanosize particles have been widely used for many catalytic processes [1–3]. In most cases, such processes were empirically discovered and optimized, involving a great deal of experimentation, and even today many of them are far from being optimized. Achieving a higher level of understanding of the reaction mechanisms and details of the catalytic processes on nanomaterials would save enormous amounts of money, and would provide useful insights for the design of alternative products.

With the advent of nanotechnology, old and new catalytic processes are being examined taking advantage of huge advances in surface science techniques and also of molecular modeling tools and methodologies [3]. There are several key points to be accounted in relation to the characterization of supported nanoparticles used in heterogeneous catalysis: (1) the exposed surfaces of the nanoparticle are far from being perfect "model catalytic surfaces"; (2) the active sites may have much higher mobilities than those in extended surfaces; (3) the nanoparticle itself may have a high mobility thus imposing a new variable: the dynamics of the process as determined by the diffusion of the supported catalytic particle; (4) the interactions of the catalyst with the substrate are crucial because strong physical, chemical, and electronic effects may radically change the nature of the catalyst; and (5) the interactions of the catalyst with the environment: gas reactants, intermediates, and products, solvent, additives, and passivating agents. All these considerations are usually ignored in molecular modeling studies of reactions on nanocatalysts, where the attention is centered on describing the chemistry of a given reaction on a model extended surface, and comparing to experiments that usually have little resemblance with the model system. In addition, the nature and details of the catalyst fabrication process are

---

* Corresponding author. Tel.: +1 979 845 3375; fax: +1 979 845 6446.
E-mail address: balbuena@tamu.edu (P.B. Balbuena).

0920-5861/$ – see front matter © 2005 Elsevier B.V. All rights reserved.
doi:10.1016/j.cattod.2005.04.012

extremely important because they determine particle morphology, particle size distribution, and interactions with the surrounding medium. For weakly interacting substrates, often a passivation agent is added to avoid particle sintering. In some cases, passivation agents arise from synthesis processes in solution, involving various classes of polymers [4] and other macromolecules that act as encapsulating agents where the metallic nanoparticle is formed [5–7].

In previous work, we have examined physical properties of nanoparticles using density functional theory and classical molecular dynamics simulations. The dependence of melting points and structural solid–solid transitions on shape and size of mono- and bimetallic nanoparticles, [8–10] as well as the influence of the substrate on the atomic distribution on bimetallic systems, [9–11] were obtained through simulated annealing procedures. Regarding the effects of a surrounding medium, it was found that an inert gas phase may cause strong changes on the shape and structure of a nanoparticle as a function of temperature and pressure, and a coupled effect of substrate and inert gas phase species may yield reversible and irreversible nanoparticle physical deformations, [12] whereas a hydrated polymer in contact with a catalytic metal nanoparticle may induce chemical and electronic transformations on the active sites, and rule the mass transfer to and from the catalytic particle [13].

Regarding synthesis of metal nanoparticles in solution, many current studies are directed to the understanding of nanoparticle formation using polymers [4,14] and to the use of macromolecules as templates [15–18]. Dendrimers in particular have been chosen as ideal systems for elucidating the process of a controlled growth of metal particles [15,18]. Polyamidoamine (PAMAM) dendrimers are branched macromolecules which are grown from a ethylenediamine core, this central core and the four branches emerging from it constitute the lowest generation dendrimer G0 (in Fig. 1, G0 would result from truncations at the N2 atoms of each branch) ending in an specific terminal group, tailored to favor particular interactions.

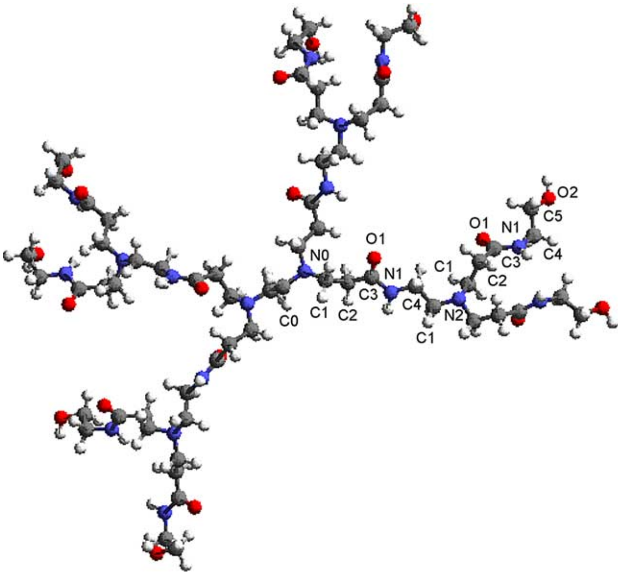

Fig. 1. Model of a PAMAM G1OH molecule. Atoms denoted C0 and N0 (tertiary amine N) belong to the ethylene-diamine core, from which four branches emerge, each one containing an amide site (atoms labeled C1, C2, C3, O1, and N1). Each of the tertiary amines (denoted as N2) constitutes the origin of two new branches repeating the amide sites and ending on a terminal group, in this case OH.

Successive generations (G1 shown in Fig. 1) add repetitive patterns growing with a tree-like structure. Using density functional theory [19,20] and classical molecular dynamics simulations [21] we have recently characterized the main interactions of PAMAM dendrimers of the lowest generations with metal ions, [19] located the active sites for attachment of neutral particles that act as seeds for nucleation and growth of metal nanoparticles, [20] and identified the main stages of the particles nucleation and growth [21]. Such complexed nanoparticles are then deposited on substrates and dried to facilitate their characterization and for catalysis tests. AFM and STM studies are however not totally unambiguous because interpreting the outcome of each of these techniques requires certain assumptions that can contribute to bias the analyses. Molecular simulations, the so-called "theoretical microscope", provide useful insights that help in the experimental interpretation. In this context we report a systematic study of the structure of naked Pt nanoparticles as a function of particle size, and the effect of dendrimer molecules on the structural properties of such supported particles. Our objective is to provide a description of

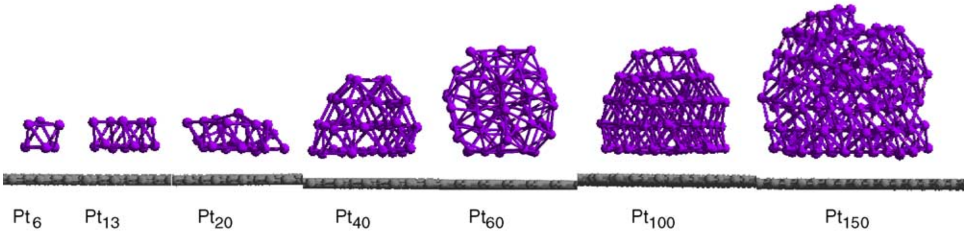

Fig. 2. Structures of Pt clusters at 300 K after simulated annealing. Most clusters show an ordered structure upon contact with the surface, except for Pt_{60}, Pt_{150}, and in lesser degree Pt_{20}.

the actual active sites in these complex nanocatalytic systems.

2. Methodology

2.1. Molecular dynamics simulation procedure

A Pt nanocluster or a Pt nanocluster with one or two dendrimer molecules were placed in a parallelepiped unit cell (49.2 × 49.2 × 50.0 Å) over a fixed slab of two graphite layers. Periodic boundary conditions were imposed in the *x*, *y*, and *z* directions. The NVT canonical ensemble was represented using the Evans thermostat to keep the temperature constant. The structure of each of the Pt_6, Pt_{13}, Pt_{20}, Pt_{40}, Pt_{60}, Pt_{100}, Pt_{150} nanoclusters deposited on a graphite surface at 300 K was optimized by energy minimization using a simulated annealing procedure. The protocol in each case consisted of starting the simulations at 600 K during 50 ps, and then the simulation temperature was decreased to 500 and 400 K with simulation lengths of 50 ps, respectively. Finally the simulation temperature was decreased to 300 K running 500 ps of equilibration time and 50 ps of production time for each nanocluster size. The simulations including dendrimers and the smallest nanoclusters, Pt_6, Pt_{13}, and Pt_{20}, were run at 300 K with 1500 ps equilibration time and 100 ps data production time for each case. The initial configurations of the dendrimers and the slabs of graphite were generated using Cerius2 [22].

2.2. Force fields

The Dreiding force field [23] was used for all the intramolecular interactions of the dendrimers which include bond stretching, angle bending, torsion, and inversion. The non-bonded interactions consist of Coulombic and Van der Waals terms. Charges of the graphite surface and Pt atoms were set to zero, and the C atoms in the substrate are fixed. The atomic charge distribution of dendrimers that determine the dendrimer-dendrimer electrostatic intermolecular interactions was taken from our previous ab initio studies [19,20]. The Lennard-Jones (LJ) 12-6 potential function [24] was used to model the non-bonded pair Van der Waals interactions. The LJ pair interactions for the dendrimer were taken from the Dreiding force field, whereas previously reported energy and length effective LJ parameters Pt–C and C–C were adopted [25,26]. The Sutton-Chen many body potential [27] was used to model the Pt–Pt interactions in the nanoclusters. Such potential has proven to yield a good performance of static and dynamic properties of transition and noble metals, such as bulk moduli and elastic constants, [27] as well as surface energies, stress tensor components and surface relaxation of fcc metals, [28] and has been used in Monte Carlo simulations to optimize transition metal cluster structures and search for their global minimum [29].

3. Results and discussion

3.1. Structure of naked Pt clusters deposited on a graphite surface

Snapshots of simulated structures for Pt_6, Pt_{13}, Pt_{20}, Pt_{40}, Pt_{60}, Pt_{100}, Pt_{150} deposited on graphite are shown in Fig. 2.

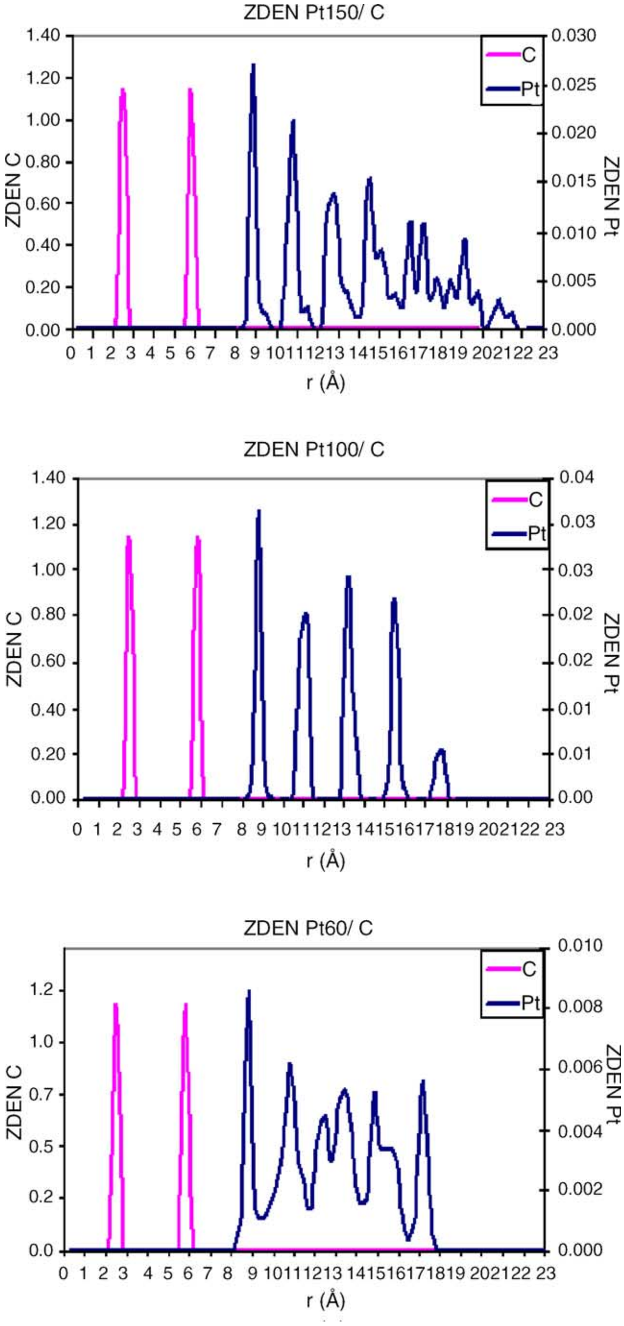

Fig. 3. Atomic distribution in the z-direction perpendicular to the substrate for Pt_{150} (top), Pt_{100} (center), and Pt_{60} (bottom) at 300 K. The pink peaks correspond to the two graphite layers (carbon density is indicated on the left vertical axis of each graph), the blue peaks are the metal cluster layers (density is indicated on the right vertical axis). The graphs are based on histograms each containing 5,000 configurations collected during MD production time.

Table 1
Vertical distances between layers, in Å, for bare clusters (shown in Fig. 2) deposited on a graphite substrate

Cluster	From first to second layer	From second layer to third layer	From third layer to fourth layer	From fourth layer to fifth layer
Pt_{20}	2.37			
Pt_{40}	2.37	2.00	2.00	
Pt_{60}	1.97	[a]	[a]	[a]
Pt_{100}	2.37	2.00	2.30	2.30
Pt_{150}	1.97	2.00	[a]	[a]

[a] Due to its amorphous characteristics, a defined distance could not be obtained.

The configurations of Pt_6, Pt_{13}, Pt_{40}, and Pt_{100} reveal an ordered layered structure, whereas those of Pt_{20} and Pt_{150} show less order, and Pt_{60} adopted a spherical shape with a small area in contact with the graphite surface.

These structural differences are manifested in the Z-density profiles displaying the atomic distribution in layers parallel to the substrate (Fig. 3), where each peak corresponds to one layer, for Pt_{60}, Pt_{100}, and Pt_{150}. Thus, the ordered structure of Pt_{100} is contrasted to that of Pt_{60} that possesses an almost spherical shape without well-defined layers except the bottom and top layers. Pt_{150} has two clear layers at the bottom of the cluster, in contact with the substrate; above these two layers the structure is more amorphous, there is a high rearrangement of Pt atoms, with some of them located in between layers.

The behavior observed in the structure of the clusters as a function of the cluster size which oscillates between ordered and less-ordered structures is the result of two aspects: (1) the competition between Pt–Pt and Pt–C interactions; (2) the total number of atoms in the cluster, that for certain sizes determines the formation of an external ‘‘atomic closed shell’’, and a clear trend towards adopting an spherical shape. The first effect definitely influences the structure of the layer in contact with the substrate, as shown by the vertical distances between layers (Table 1), which indicate that the bottom sections of the ordered clusters (Pt_{20}, Pt_{40}, and Pt_{100}) adopt a hcp structure to match the hexagonal graphite structure. The value of 2.37 Å is in agreement with the interlayer separation estimated to have a ratio $c/a = 1.633$, with a the Pt–Pt bond distance in one layer, and c the distance between A and A layers in a ABA hcp structure [30]. Note however, that the smaller value of 2 Å found in the upper interlayers of Pt_{40} and in the second interlayer of Pt_{100} suggests that the fcc structure is recovered in the top layers for Pt_{40} and in the middle layers for Pt_{100}. The vertical distances for the top two interlayers of Pt_{100} are also in agreement with an hcp structure. Similar mixing of fcc and hcp structures in small clusters was recently reported [31]. In the less ordered structures Pt_{60} and Pt_{150}, the smaller interlayer separations of 1.97 and 2 Å respond to an fcc pattern.

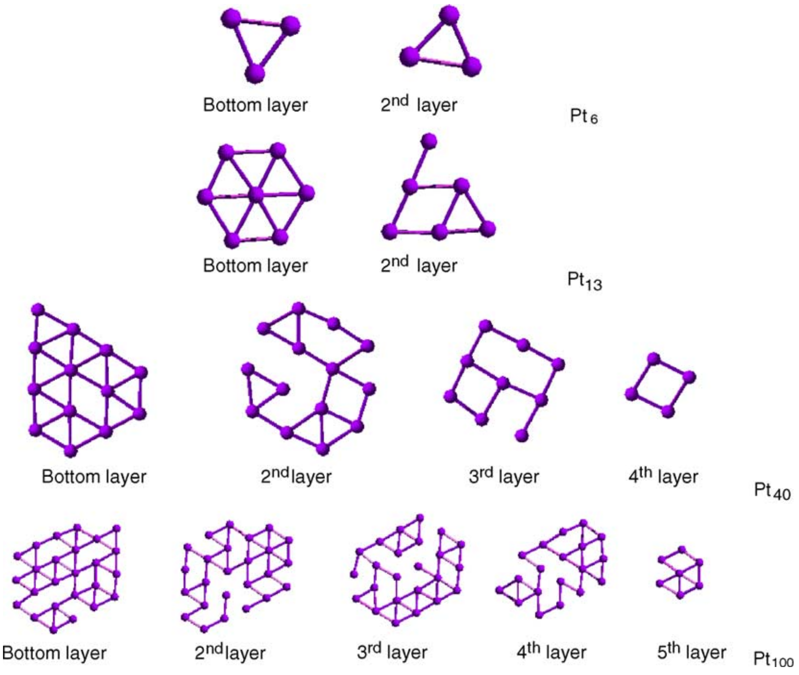

Fig. 4. Layer-by-layer structure of Pt_6, Pt_{13}, Pt_{40}, and Pt_{100}. In each case, the bottom layer is the one in contact with the substrate. Atoms are shown disconnected from each other when their bond length exceeds a certain threshold. This structure corresponds to a snapshot obtained after system equilibration.

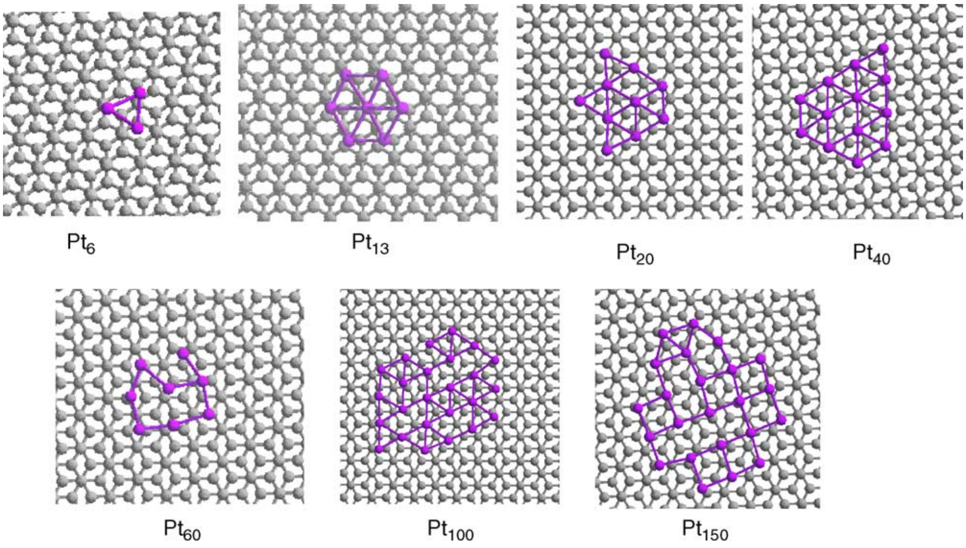

Fig. 5. Layers of Pt clusters in contact with graphite surface. The cluster attachment to the surface tries to maximize the contact with the C atoms, in some cases (Pt_{60} and Pt_{150}) changing the geometrical arrangement of the Pt atoms in that layer. These structures correspond to snapshots obtained after system equilibration.

Fig. 4 illustrates the layer-by-layer structures of Pt_6, Pt_{13}, Pt_{40}, and Pt_{100}. The atoms in each layer in Pt_6, Pt_{13} and Pt_{100} accommodate according to a hexagonal lattice. For Pt_{40} except the bottom layer that follows the hexagonal pattern, the other layers mainly form a rectangular lattice, another indication of the mixing of fcc and hcp patterns in this cluster. The atomic distribution in the various layers shows the evolution of the cluster shape from an almost two-dimensional (Pt_6, Pt_{13}) to a three-dimensional structure in the larger clusters.

Fig. 5 shows the contact between the graphite surface and the bottom layer of each Pt cluster. The average distance between Pt atoms in the bottom layer is 2.66 Å for Pt_{20} and Pt_{40}, 2.75 Å for Pt_{60}, 2.69 Å for Pt_{100}, and 2.75 Å for Pt_{150}. The change from 2D to 3D is clearly seen by counting the number of atoms in the bottom layer, there is 50% of the total number of Pt atoms in the smallest clusters (Pt_6, Pt_{13}, and Pt_{20}), and 25% in the cases where a 3D ordered phase is established such as Pt_{40} and Pt_{100}. The exceptions are Pt_{60} that has only 10% of its total number of atoms in the bottom layer, and Pt_{150}, with about 15%, and in these two cases, the structure of the bottom layer evolves to a rectangular lattice, in an effort to maximize the interactions with the substrate atoms while the overall structure tends to a spherical shape.

Our previous simulation results showed that the presence of a gas pressure acting on the nanocluster surface favored this conformational evolution (from hexagonal to rectangular lattice) for the bottom layer in contact with the substrate [12]. These new results indicate that this morphology change is also related to the size of the Pt particle. Overall, the average distance among the nearest neighboring Pt atoms increases with the number of atoms in the cluster increasing, as illustrated in Fig. 6 by the radial distribution function $g_{Pt-Pt}(r)$. The largest clusters have average distances close to those found in the bulk Pt crystal, approximately 2.75 Å.

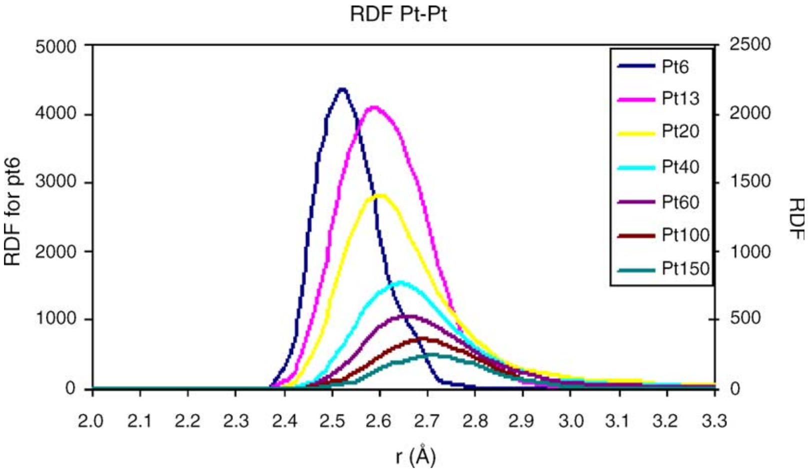

Fig. 6. Pt–Pt radial distribution functions in the clusters. The scale on the left vertical axis is for the g(r) of the smallest cluster, Pt_6, all the other g(r) values are shown on the right vertical axis. The shift in the peak position shows the increase of the Pt–Pt average distance with increasing cluster size.

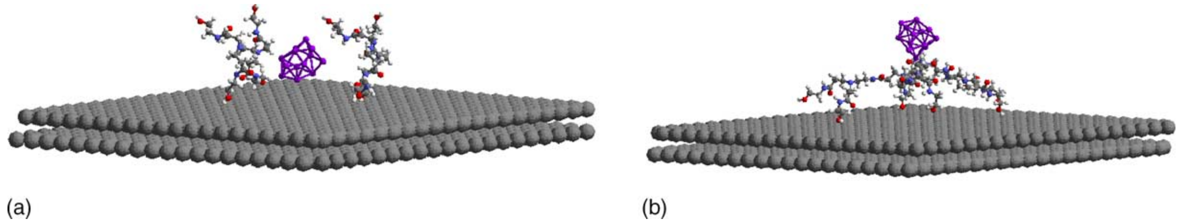

Fig. 7. Initial configurations of Pt_{13} (a) with two G0OH molecules; (b) with G1OH molecule.

3.2. Interactions dendrimers/Pt clusters/graphite

We investigated the interactions of the smallest clusters Pt_6, Pt_{13}, and Pt_{20} with one or two molecules of G0OH and with one molecule of G1OH on the graphite surface. The metal cluster size generated inside of a given dendrimer depends on the dendrimer size, and therefore on its number of attractive sites [18,32,33]. However, in the post-processing after the synthesis, the exact location of the metal clusters is still debated, i.e., they could keep enclosed in the template or being outside the template but attached to branches of other dendrimer molecules different than their original cage. Thus, our objective is to analyze how dendrimer branches would interact with Pt particles, and what would be the effect of the macromolecules on the nanocluster structures once the generated particles are ready to act as catalysts.

Initial configurations were generated using the annealed structures of the respective Pt clusters and adding one or two dendrimer molecules to the cell containing the graphite surface. Fig. 7 gives examples of the initial configurations of Pt_{13} with two G0OH molecules and the same cluster Pt_{13} with one G1OH molecule. These initial configurations were the result of minimizing the energy of the complete system previous to the MD runs.

The structures displayed in Fig. 7 were selected to illustrate that the main features of the interactions dendrimers/Pt clusters/graphite are independent of the initial configurations. Both G0OH and G1OH dendrimers extend openly on graphite adopting a flat structure with two branches belonging to one of the G0OH molecules (Fig. 8a) and two branches from G1OH (Fig. 9a) surrounding the sides of Pt_6, reflecting a competition between dendrimer–dendrimer, dendrimer–Pt, and dendrimer–substrate interactions.

Neither Fig. 8a nor Fig. 9a show dendrimer branches crossing over the metal nanoparticle. In the first case, the Pt atoms are attracted by the OH terminal groups (O2 in the

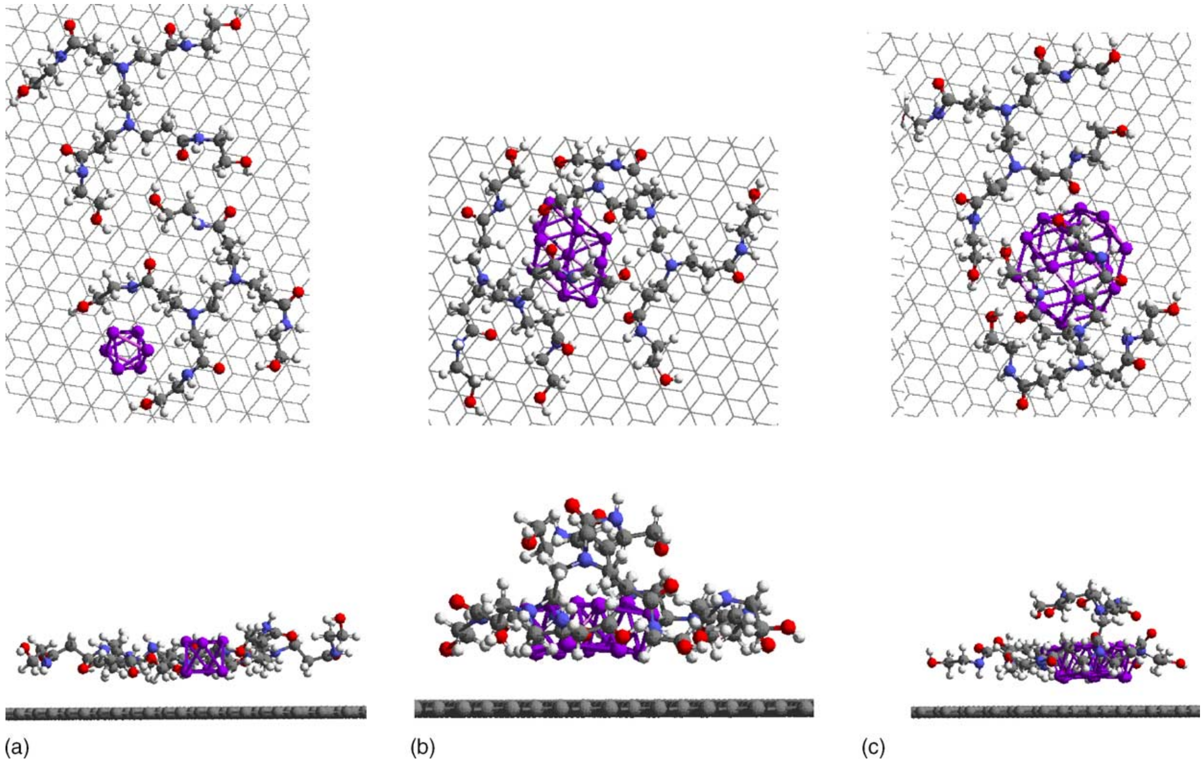

Fig. 8. Snapshots obtained after system equilibration for (a) Pt_6-2G0OH, (b) Pt_{13}-2G0OH, and (c) Pt_{20}-2G0OH. Top views on top, side views at the bottom.

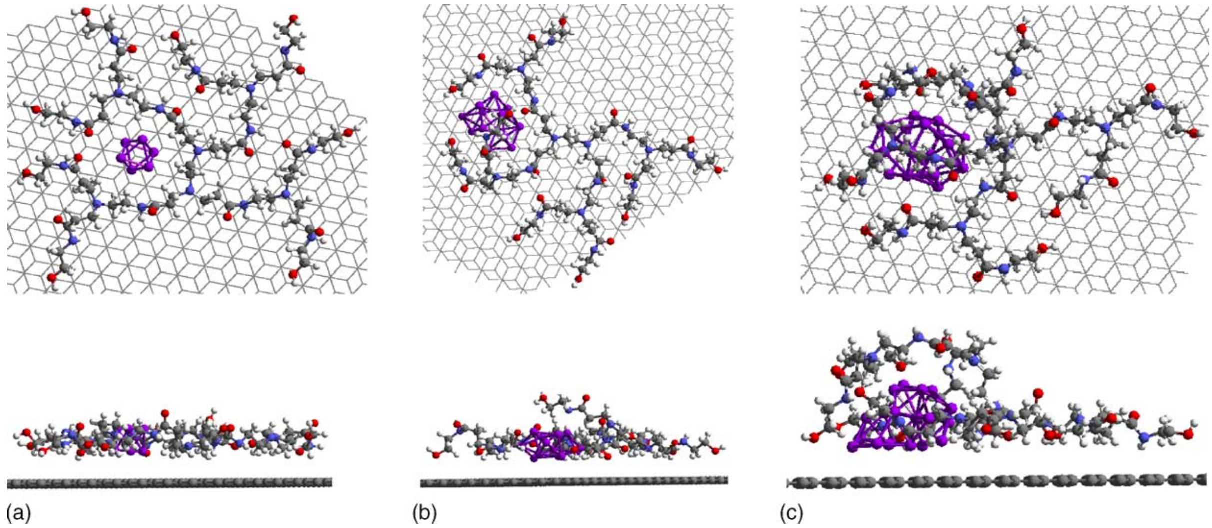

Fig. 9. Snapshots obtained after system equilibration for (a) Pt_6-G1OH, (b) Pt_{13}-G1OH, and (c) Pt_{20}-G1OH. Top views on top, side views at the bottom.

nomenclature of Fig. 1), by the amide N atoms (N1), and by the core tertiary amine N atoms of G0OH (N0), whereas the amide O atoms (O1) are involved in intra and intermolecular interactions of their own or a from a neighbouring dendrimer molecule. In the case of G1OH (Fig. 9a) the Pt_6 atoms interact with the amide oxygen atoms but not with the OH groups, since the inner branches of G1OH are the ones that surround the particle, the ''caging'' is also favored by intramolecular interactions as seen from Fig. 9a.

In contrast to Pt_6, Pt_{13} is completely surrounded by branches of both G0OH molecules (Fig. 8b) on the surface of graphite and a few branches cross over the Pt particle (Fig. 8b, side view). Similarly, two branches of G1OH enclose the particle (Fig. 9b) and one of the end branches crosses over the particle (side view). Thus, as the particle size increases, the dendrimer branches form a 'cage' (see Pt_{20} in Figs. 8c and 9c), which indicates that the interaction Pt cluster/dendrimer starts to win over the dendrimer–

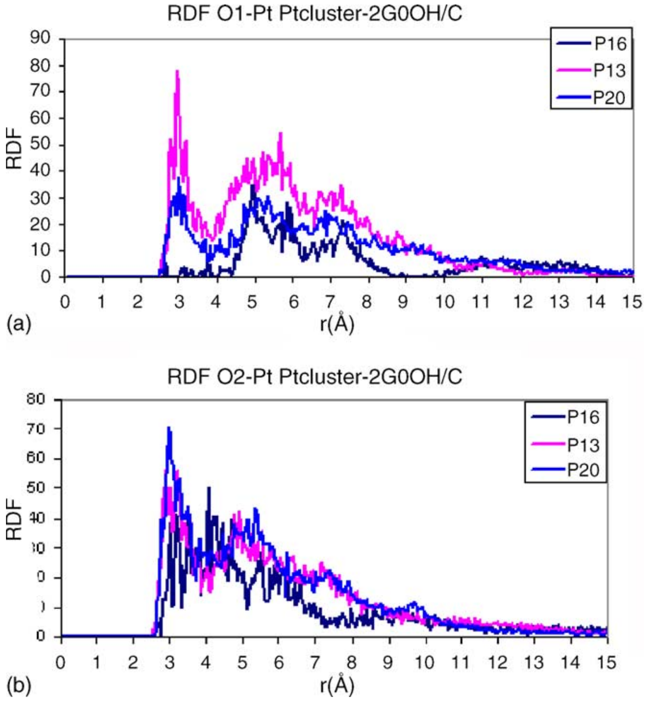

Fig. 10. Radial distribution function of G0OH oxygen atoms interacting with Pt in Pt clusters deposited on graphite. (a) $g_{O1Pt}(r)$, where O1 is an interior amide oxygen, (b) $g_{O2Pt}(r)$, where O2 is a terminal oxygen atom from the OH group. Two dendrimer molecules are present in the simulation box.

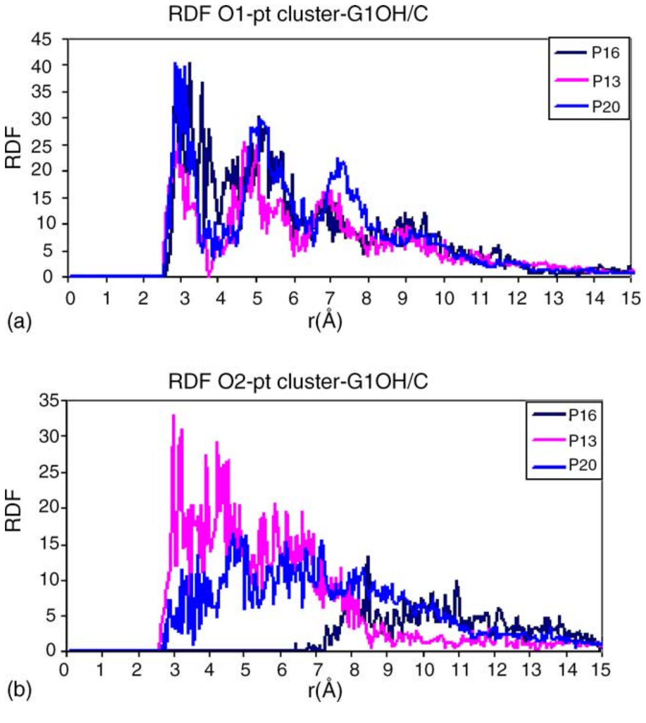

Fig. 11. Radial distribution function of oxygen with Pt in Pt clusters with G1OH deposited on graphite. (a) $g_{O1Pt}(r)$, where O1 is an interior amide oxygen, (b) $g_{O2Pt}(r)$, where O2 is a terminal oxygen atom from the OH group.

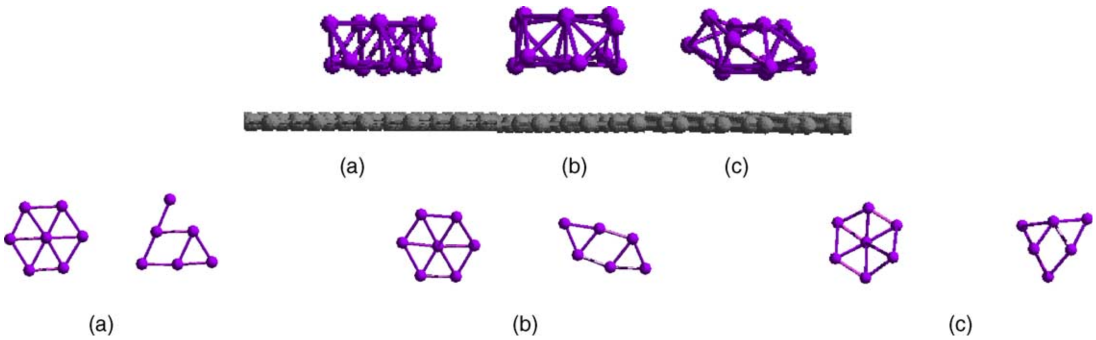

Fig. 12. Pt_{13} overall and layer-by-layer structure on graphite. For clarity, dendrimers are not shown in cases b and c. (a) Pt_{13} without dendrimer on graphite; (b) Pt_{13} with 2G0OH on graphite; (c) Pt_{13} with G1OH on graphite. Left layer in each case is the bottom layer. Structures correspond to snapshots obtained after system equilibration.

dendrimer and intradendrimer interactions. The small size of Pt_6 does not cause too much bending in the dendrimer branches that prefer to remain involved with intramolecular interactions and interactions with the surface atoms.

Details of the interactions that complement and confirm those observed from the instantaneous snapshots are given by the radial distribution functions (RDF) between Pt atoms and dendrimers displayed in Figs. 10 and 11. We focus on the interactions between Pt atoms and the interior amide oxygen (O1Pt) and between Pt and peripheral hydroxyl oxygen atoms (O2Pt). Our own ab initio studies [19,20] and the experimental literature [17,34] suggest that the metal ions selectively coordinate to interior amide group in hydroxyl-terminated PAMAM prior to the nanoparticle formation. Another report indicated the direct involvement of the dendrimer C=O group with the Pt particle [35]. Simulations of the formation of metal nano-particle on hydroxyl-terminated PAMAM showed similar results [21]. In agreement with the observations from Figs. 8a and 9a, comparison of the positions of the first peak for Pt_6 in Fig. 10a and b indicates that the Pt atoms are ~3–4 Å closer to the O2 terminal than to the O1 amide atom in their interaction with G0OH. In the larger clusters, the PtO1 first peak becomes sharp and well-defined, and a bit closer to the Pt atoms than that of PtO2.

For G1OH (Fig. 11) the interactions between O1 and Pt are stronger than those between O2 and Pt which is consistent with the results from Figs. 8 and 9, i.e., the interactions between graphite and the Pt atoms are strong enough to retain the particle attached to its surface, but can not overcome the strength of the attraction between the Pt particle and the surrounding dendrimer branches. That means the interactions Pt cluster/dendrimer are strong enough to isolate the particle preventing sintering.

3.3. *Dendrimer effects on the structure of the Pt nanoparticles*

Simulation results (Figs. 8a and 9a) indicate that for Pt_6, neither G0OH nor G1OH have apparent impact on the nanoparticle structure and Pt_6 keeps its two-layer structure shown in Figs. 2 and 4. For Pt_{13} and Pt_{20}, the structures of the nanoparticles have dramatic changes compared to those without dendrimers. Though the presence of two G0OH molecules did not change the two-layer structure of Pt_{13}, the Pt atoms in the top layer rearranged (Fig. 12b). When Pt_{13} is deposited on graphite with G1OH, the final configuration does not have a well-defined layer-by-layer structure,

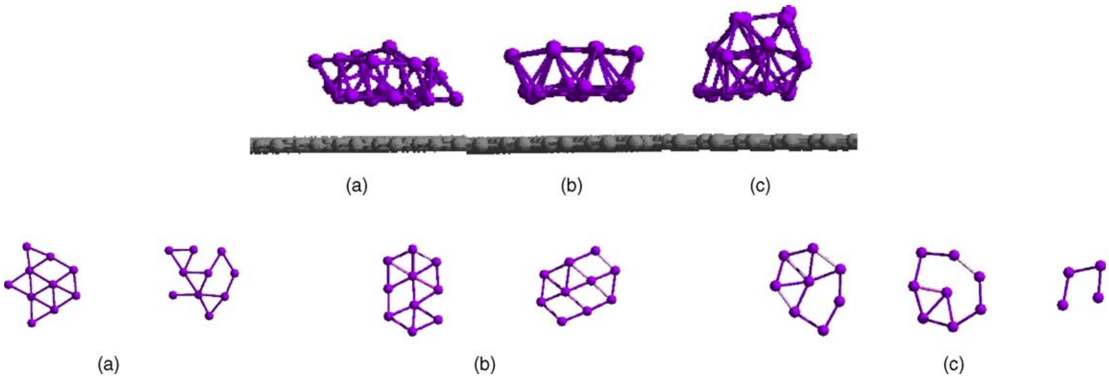

Fig. 13. Pt_{20} overall and layer-by-layer structure on graphite. For clarity, dendrimers are not shown in cases b and c. (a) Pt_{20} without dendrimer on graphite; (b) Pt_{20} with 2G0OH on graphite; (c) Pt_{20} with G1OH on graphite. Left layer in each case is the bottom layer. Structures correspond to snapshots obtained after system equilibration.

although it can be roughly divided into two layers (Fig. 12c). The hexagonal-lattice structure of each layer in Pt_{13} is still preserved.

Both dendrimers strongly impact the morphology of the larger Pt_{20} cluster. In the case of Pt_{20} with G0OH (Fig. 13b), the arrangements of Pt atoms in both the bottom and top layers are different from those without dendrimer and the two-layer structure is still kept. But when Pt_{20} interacts with G1OH on graphite its conformation adopts a rough three-layer structure which is quite different from the other two Pt_{20} cases. The hexagonal structure of each layer is not perfectly preserved.

The effects of G0OH and G1OH on the structure of Pt_{20} on the graphite surface are clearly shown in Fig. 14, where the three-dimensional structure is evident in Fig. 14c. Since the density profiles shown in Fig. 14 are averages over many configurations, they confirm that the instantaneous snapshots are representative of stable structures. Therefore, higher generation dendrimers with larger number of active sites have stronger effects on the morphology of Pt nanoparticles than those produced by lower generation dendrimers, and the largest Pt nanoparticles are more sensitive to the template effect.

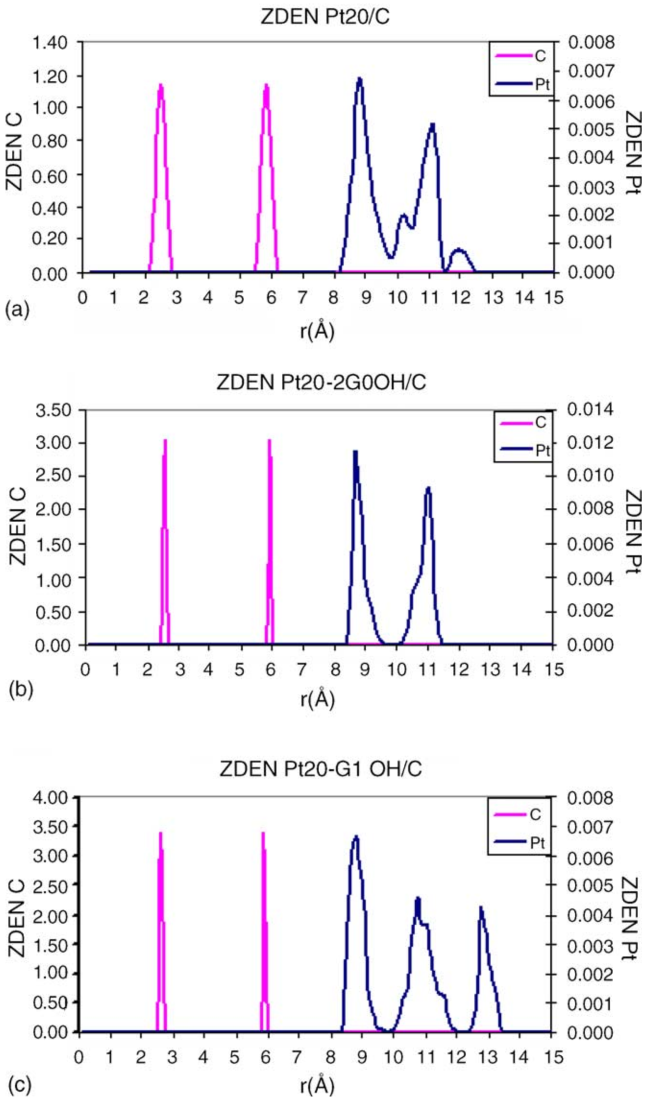

Fig. 14. Z-density profile of Pt_{20} deposited on graphite. (a) without dendrimer; (b) Pt_{20} with 2 G0OH molecules; (c) Pt_{20} with G1OH. The right vertical axis represents the atomic density of C atoms in graphite, the left vertical axis indicates the atomic density of Pt atoms in the cluster. The graphs are based on histograms each containing 5000 configurations collected during MD production time.

4. Conclusions

Even a weakly interactive substrate as graphite exerts a strong influence on the structure of metal nanoparticles, and such influence is a function of the nanoparticle size, with variations following an oscillatory pattern according to the degree of completeness of the particle's outer atomic shell. Small nanoparticles (Pt_6, Pt_{13}, Pt_{20}) adopt a quasi-two-dimensional structure, and the atoms in the layer in contact with the surface arrange in the hexagonal lattice tending to maximize the interactions with the graphite substrate. The simulation results for Pt_{100} suggest the existence of mixed fcc and hcp structures, with hcp layers located in contact with the substrate and in the upper layers, and the fcc structure in the middle. The structure is similar for Pt_{40} although it lacks the top hcp structure. Less ordered structures (Pt_{60}, Pt_{150}) show a tendency of the nanoparticle to adopt a spherical shell, with a small layer in contact with the substrate adopting a rectangular pattern.

Details of the particle morphology, atomic distribution, and interactions of Pt_6, Pt_{13}, and Pt_{20} with the substrate in the presence of the dendrimers are compared with those for the bare nanoparticles deposited on graphite. Simulation results reveal a strong attachment of the dendrimer branches to the metal particle; the binding is mainly driven by the oxygen and nitrogen amide atoms, the interior tertiary amines, and the dendrimer terminal groups. Such attachment has significant effects on the structure of Pt nanoparticles on graphite surfaces, manifested by atomic rearrangements in the metal clusters causing modifications to their initial fcc structure and the appearance of new layers. Compared to the smaller G0OH, G1OH yields more obvious effects and the largest Pt particles are more easily affected.

In summary, this work shows that both substrate and surrounding medium exert significant effects on the morphology and crystalline structure of metal nanoparticles, and that the extent and characteristics of such effects depend on particle size and nature of the substrate and surrounding medium. Changes in morphology and crystal structure will also induce specific electronic effects on the clusters, which in turn modify their chemical properties and consequently affect their catalytic performance.

Acknowledgements

This work is supported by the National Science Foundation grant CTS-0103135. Supercomputer resources granted by the National Energy Research Scientific Computing Center (NERSC), by the DoD Major Shared Resource Centers (ARL MSRC and ASC MSRC), and by the National Center for Supercomputer Applications under grant CTS040003 are gratefully acknowledged.

References

[1] B.F.G. Johnson, Top. catal. 24 (2003) 147.
[2] J. Schicks, N. D., S. U., V. G., Catal. today 81 (2003) 287.
[3] P.L. Gai, R. Roper, M.G. White, Curr. Op. Sol. St. Mater. Sci. 6 (2002) 401.
[4] A.K. Sra, R.E. Schaak, J. Am. Chem. Soc. 126 (2004) 6667.
[5] K. Esumi, Top. Curr. Chem. 227 (2003) 31.
[6] J.M.J. Frechet, J. Polym. Sci. Part A: Polym. Chem. 41 (2003) 3713.
[7] R.M. Crooks, B.I. Lemon III, L. Sun, L.K. Yeung, M. Zhao, Top. Curr. Chem. 212 (2001) 81.
[8] S.-P. Huang, P.B. Balbuena, Mol. Phys. 100 (2002) 2165.
[9] S.-P. Huang, P.B. Balbuena, J. Phys. Chem. B 106 (2002) 7225.
[10] S.-P. Huang, D.S. Mainardi, P.B. Balbuena, Surf. Sci. 545 (2003) 163.
[11] S.R. Calvo, P.B. Balbuena, Surf. Sci (2004), submitted for publication.
[12] E.J. Lamas, P.B. Balbuena, J. Phys. Chem. B 107 (2003) 11682.
[13] P.B. Balbuena, E.J. Lamas, Y. Wang, J. Electrochim. Acta (2004), submitted for publication.
[14] P. Schuetz, F. Caruso, Chem. Mater. 16 (2004) 3066.
[15] L. Balogh, D. Tomalia, J. Am. Chem. Soc. 120 (1998) 7355.
[16] C. Bao, M. Jin, R. Lu, T. Zhang, Y.Y. Zhao, Mater. Chem. Phys. 81 (2003) 160.
[17] L. Balogh, R. Valluzzi, K.S. Laverdure, S.P. Gido, G.L. Hagnauer, D.A. Tomalia, J. Nanoparticle Res. 3 (1999) 1.
[18] R.M. Crooks, M. Zhao, L. Sun, V. Chechik, L.K. Yeung, Acc. Chem. Res. 34 (2001) 181.
[19] F. Tarazona-Vasquez, P.B. Balbuena, J. Phys. Chem. B 108 (2004) 15992.
[20] F. Tarazona-Vasquez, P.B. Balbuena, J. Phys. Chem. B 108 (2004) 15982.
[21] F. Tarazona-Vasquez, P.B. Balbuena, AIChE National Meeting, Austin, TX, 2004.
[22] MSI. Force-field based simulations San Diego, 1997.
[23] S.L. Mayo, B.D. Olafson, W.A. Goddard, J. Phys. Chem. 94 (1990) 8897.
[24] M.P. Allen, D.J. Tildesley, Computer Simulation of Liquids;, Oxford University Press, Oxford, 1990.
[25] G.-W. Wu, K.-Y. Chan, Surf. Sci. 365 (1996) 38.
[26] G.-W. Wu, K.-Y. Chan, J. Electroanal. Chem. 450 (1998) 225.
[27] A.P. Sutton, J. Chen, Philos. Mag. Lett. 61 (1990) 139.
[28] B.D. Todd, R.M. Lynden-Bell, Surf. Sci. 281 (1993) 191.
[29] J.P.K. Doye, D.J. Wales, New J. Chem. (1998) 733.
[30] W.D. Callister, Materials science and engineering: An introduction, John Wiley & Sons Inc., New York, 1994.
[31] Y.H. Chui, K.Y. Chan, Phys. Chem. Chem. Phys. 5 (2003) 2869.
[32] P.J. Pellechia, J.X. Gao, Y.L. Gu, H.J. Ploehn, C.J. Murphy, Inorg. Chem. 43 (2003) 1421.
[33] M. Zhao, R.M. Crooks, Adv. Mater. 11 (1999) 217.
[34] L. Balogh, D.A. Tomalia, G.L. Hagnauer, Chem. Innovation 30 (2000) 19.
[35] D. Liu, J. Gao, C.J. Murphy, C.T. Williams, J. Phys. Chem. B 108 (2004) 34.